www.sciencemag.org/cgi/content/full/science.aai9127/DC1

Supplementary Materials for

Translational termination without a stop codon

Nathan R. James, Alan Brown, Yuliya Gordiyenko, V. Ramakrishnan*

*Corresponding author. Email: ramak@mrc-lmb.cam.ac.uk

Published 1 December 2016 on *Science* First Release
DOI: 10.1126/science.aai9127

This PDF file includes:

Materials and Methods

ArfA purification

A pET16b vector encoding *E. coli* ArfA with a twelve-residue C-terminal truncation and a decahistidine N-terminal tag followed by a Factor Xa cleavage site was a kind gift from Dr. Yoshihiro Shimizu (RIKEN). The protein was expressed in *E. coli* BL21 (DE3) cells (Novagen) for 4 h at 37 °C after induction at OD_{600} 0.5 with a final concentration of 1 mM IPTG. The cells were resuspended and lyzed by sonication in lysis buffer (50 mM HEPES–KOH (pH 7.5), 1 M NH_4Cl, 5 mM $MgCl_2$, 40 mM imidazole and 6 mM 2-mercaptoethanol) and applied to a HisTrap column (GE Healthcare). The protein was eluted over a gradient up to 1 M imidazole before being dialyzed overnight against dialysis buffer (50 mM HEPES–KOH (pH 7.5), 50 mM KCl, 5 mM $MgCl_2$, 2 mM $CaCl_2$ and 6 mM 2-mercaptoethanol) containing Factor Xa (NEB). Untagged ArfA was obtained by passing the solution through a HisTrap column. ArfA was purified further by size-exclusion chromatography with a Superdex 75 16/600 column (GE Healthcare) equilibrated with buffer G (5 mM HEPES–KOH (pH 7.4), 50 mM KCl, 10 mM NH_4Cl, 10 mM $Mg(OAc)_2$ and 6 mM 2-mercaptoethanol). ArfA(A18T) was prepared following the same procedure.

Sample preparation and electron cryomicroscopy

E. coli 70S ribosomes were purified as described previously (*31*). *T. thermophilus* RF2 (TtRF2) was purified as described (*16*). Dr. Ramanujan S. Hegde (MRC LMB) provided His-tagged *E. coli* RF2 from the PURE system (*32*). *E. coli* fMet-NH-$tRNA^{fMet}$ containing a nonhydrolyzable amide bond between A76 and the *N*-formylmethionine was prepared as described (*33*). A truncated version of Z4C mRNA (*34*) that ends immediately after the AUG start codon was chemically synthesized (GE Dharmacon).

Reaction mixtures of 500 µl were prepared in buffer G containing 130 nM *E. coli* 70S ribosomes. The mixtures were incubated for 5 min at 37 °C after addition of each of the following components: 520 nM mRNA, 1.3 µM fMet-NH-$tRNA^{fMet}$, 1.3 µM wild-type ArfA, and either 1.3 µM RF2 or TtRF2. Additional reactions were prepared with 3.2 µM ArfA(A18T) and 1.3 µM RF2, and with 1.3 µM wild-type ArfA but lacking RF2. The mixtures were then held on ice before being frozen onto grids.

UltrAuFoil R 1.2/1.3 grids (for the complex with TtRF2) and QUANTIFOIL R 2/2 grids (for the other complexes) were coated with a continuous carbon film (~60 Å in thickness) and glow-discharged for 30 s at 6 V. Aliquots of 3 µl of reaction mixture were incubated on the grids for 30 s at 4 °C and 100% humidity. The grids were then blotted for 4 to 5 s and flash-frozen in liquid ethane using a Vitrobot Mark III (FEI).

Micrographs were collected using a Titan Krios microscope at 300 keV with a Falcon II detector and EPU software (all FEI). A dose rate of 40 $e \cdot Å^{-2} \cdot s^{-1}$ was used. The defocus values ranged from –2.0 to –3.0 µm, the exposures were 1.2 s with 20 movie frames and the calibrated magnification of 134,615× resulted in a pixel size of 1.04 Å.

Image processing

The movie frames of each image were aligned using MotionCorr (*35*). Parameters of the contrast transfer function were obtained using Gctf (*36*) for each motion-corrected micrograph. All subsequent processing was performed in RELION-2.0 (*37*), except for the dataset with TtRF2, which was processed in RELION-1.4. Semiautonomous particle picking (*38*) was used to select ribosomes from the micrographs. Incorrectly selected nonribosomal particles were discarded after reference-free two-dimensional classification. A cryo-EM map of the 70S–RelA complex (EMD-8107) (*31*), low-pass-filtered to 40 Å, was used as an initial reference for the first three-dimensional refinement. An initial round of three-dimensional classification without further aligning the particles was used to discard empty 70S ribosomes, free 50S subunits and poorly aligned particles (Fig. S1). After another refinement, motion correction was performed for each particle using a running average of three movie frames and a standard deviation of one pixel for the translational alignment. In addition, each frame was weighted with a B-factor to compensate for radiation damage. After this "particle-polishing" step, focused classification with signal subtraction (FCwSS) (*39*) was used to isolate particles containing ArfA and RF2 (or an empty A site for the dataset without RF2). An additional three-dimensional classification without alignments and two rounds of FCwSS were performed on the dataset with TtRF2 to improve the quality of the map. For the other datasets, a final three-dimensional classification with local angular searching was performed as a final clean-up of the data. Despite multiple

rounds of classification, no ArfA was visible in the dataset without RF2. This dataset was used to model a nonstop complex with an unoccupied A site.

The final statistics for each dataset are given in Table S1. Reported resolutions are based on the Fourier-shell-correlation (FSC) 0.143 criterion (*40*). High-resolution noise substitution was used to correct for the effects of applying a mask during the FSC calculations (*41*). Before visualization, density maps were corrected for the modulation transfer function of the Falcon II detector and sharpened by applying a negative B-factor that was estimated using automated procedures (*40*). Local resolution was quantified using ResMap (*42*) (Fig. S2).

Model building

Models of the *E. coli* 70S ribosome and fMet-tRNA^{fMet} (*31*) were docked into the maps using Chimera (*43*) and each chain was subsequently rigid-body-fitted in Coot (*44*). All chains were manually adjusted to fit the density. The crystal structures of *E. coli* RF2 (PDB accession code 1GQE) (*21*) and TtRF2 (PDB accession code 2IHR) (*23*) were rigid-body-fitted into the A site and partially rebuilt to fit the densities. ArfA was built *de novo*.

Model refinement and validation

Reciprocal-space refinement was carried out in REFMAC v5.8 optimized for cryo-EM maps using external restraints generated by ProSMART and LIBG (*45*). The fit of the model to the map density was quantified using $FSC_{average}$ (*45*) and CRef (*40*). CRef is a measure of the resolution when the FSC between the refined model and map is 0.5, and should closely agree with resolution of the map by the FSC=0.143 criterion (*40*). Model statistics were obtained using MolProbity (*46*) and provided in Table S1. Cross-validation against overfitting was performed as previously described (*45*) (Fig. S2A).

All figures were created using PyMOL (*47*) or Chimera (*43*).

Supplementary Figures

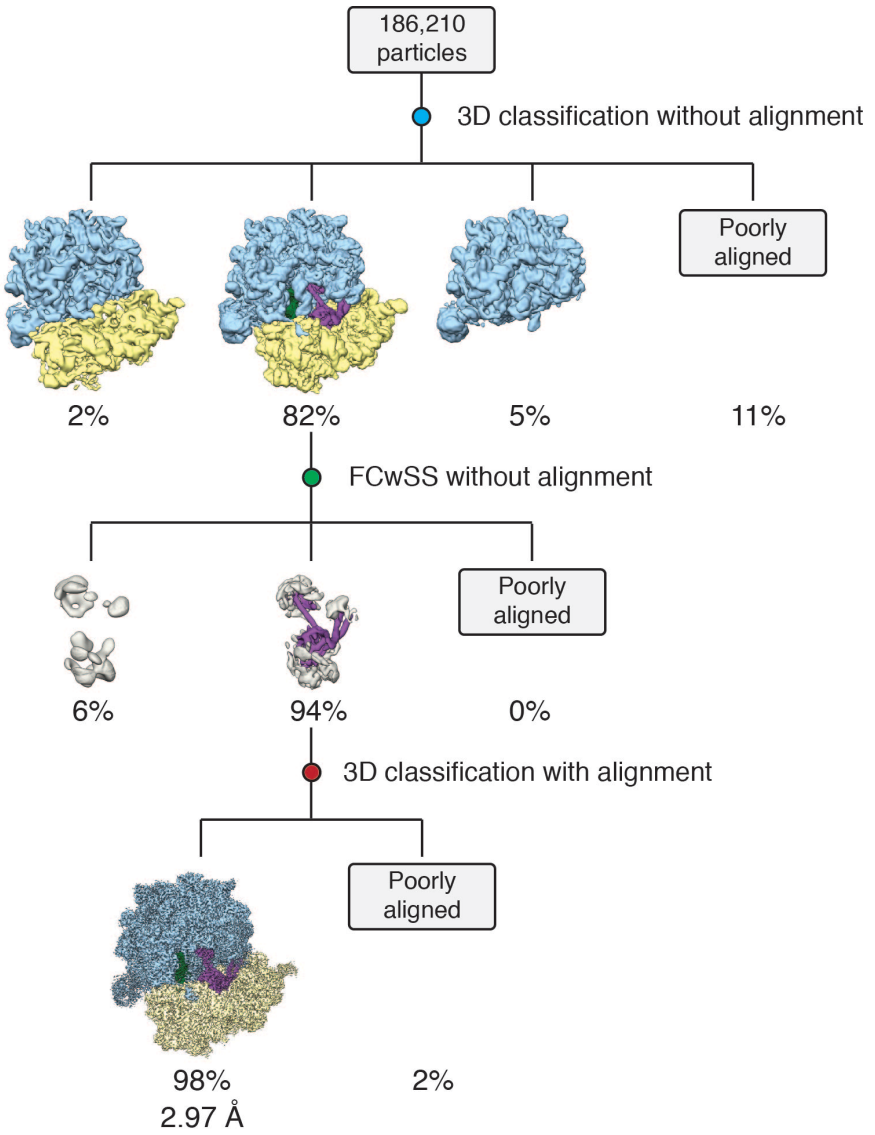

Fig. S1. *In-silico* classification. Three rounds of *in-silico* classification were used to isolate a single well-defined map for the nonstop complex recognized by wild-type ArfA and RF2. 186,210 particles selected from 2D classification were classified while preserving the Euler angles from a prior 3D refinement step. This separated nonstop complexes from empty ribosomes, isolated 50S subunits and poorly aligned particles. FCwSS using a mask over RF2 removed further empty ribosomes. A final 3D classification, this time allowing angular sampling, removed any remaining poorly aligning particles. The final reconstruction has a nominal resolution of 2.97 Å. All other datasets were classified similarly, with any changes to the scheme described in the methods.

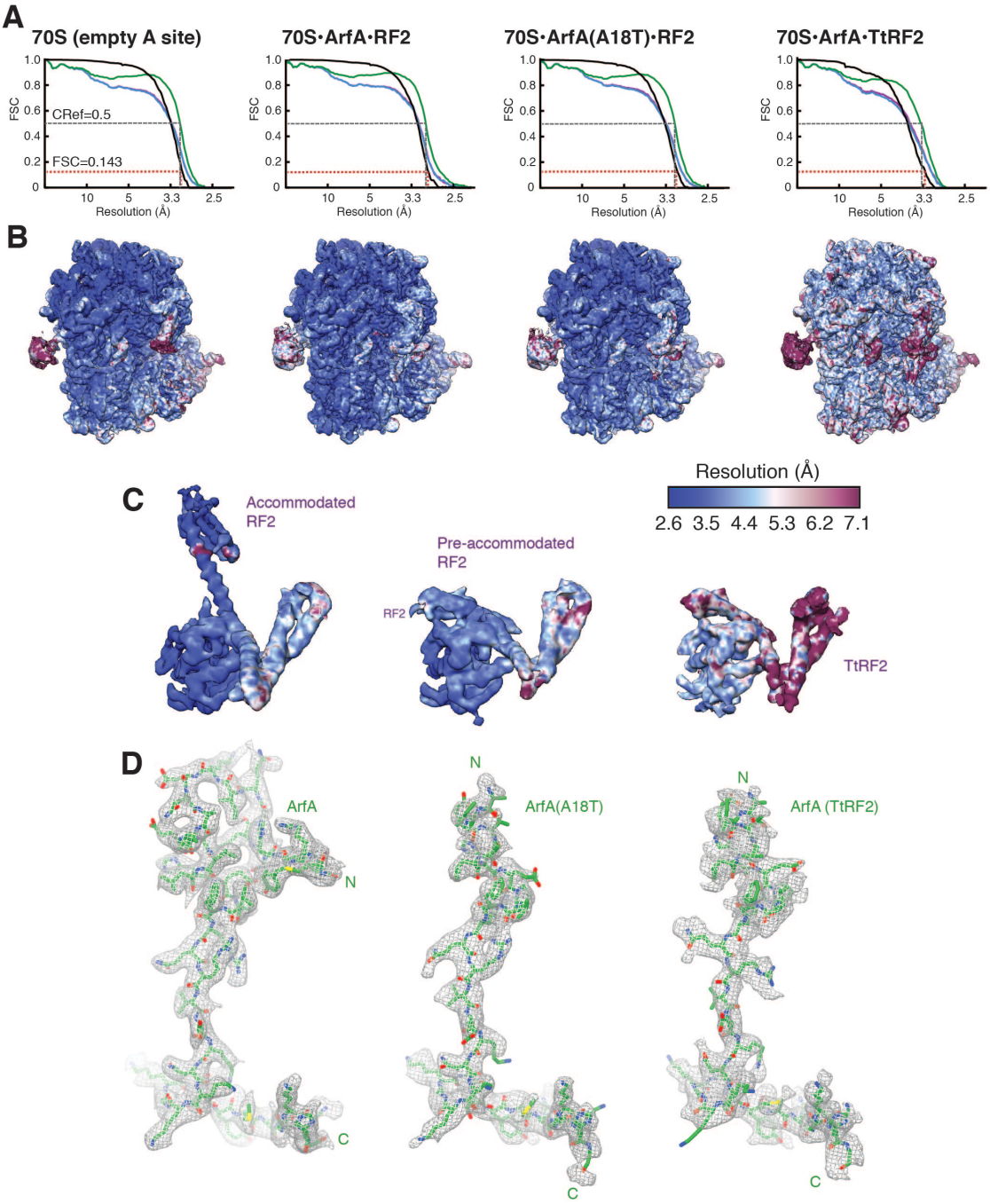

Fig. S2. Quality of maps and models. (**A**) Fourier-shell-correlation (FSC) curves for each reported cryo-EM reconstruction (black). The resolution at FSC=0.143 is indicated with a red dashed line. Also shown are FSC curves of the fit of the refined model to the final map (green) for each structure. The resolution at FSC=0.5 (CRef) is indicated with a grey dashed line. The self- and cross-validated correlations are shown in purple and blue, respectively. (**B**) The cryo-EM map for each complex is colored by local resolution. (**C**) Isolated density for RF2 and TtRF2 colored by local resolution for each complex. (**D**) Density and model for ArfA from each complex.

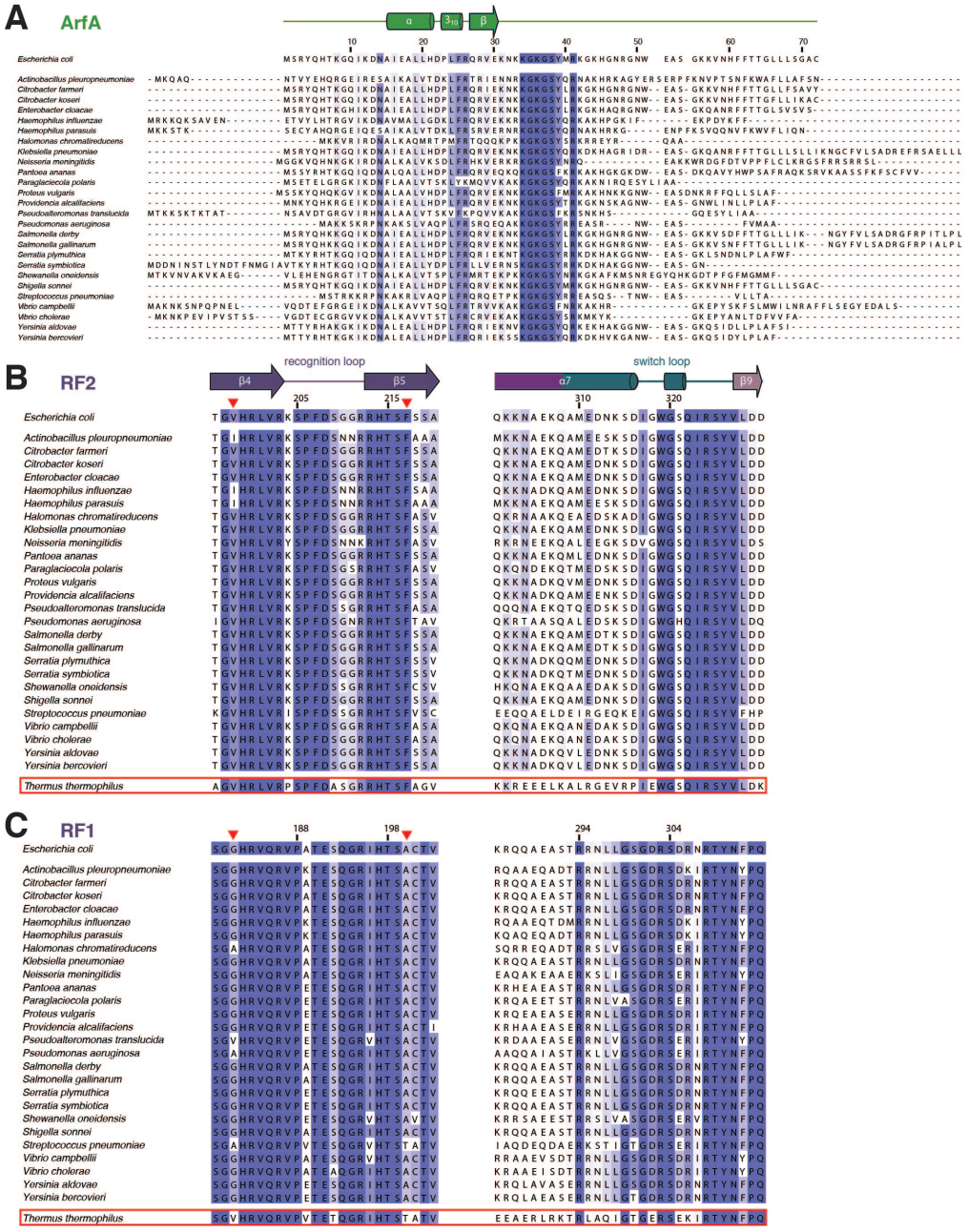

Fig. S3. Sequence alignments. (**A**) Alignment of selected ArfA sequences. Numbering and secondary structure corresponds to *E. coli* ArfA. (**B**) Alignment of the recognition and switch loops of RF2 from ArfA-containing species and from *T. thermophilus*, which lacks an ArfA ortholog. Numbering and secondary structure corresponds to *E. coli* RF2. Hydrophobic residues that confer specificity for ArfA are indicated with arrowheads. (**C**) Alignment of the recognition and switch loops of RF1. The numbering corresponds to *E. coli* RF1. All sequences were obtained from UniProt (*48*), aligned with MUSCLE (*49*) and visualized in Jalview (*50*). Residues are colored only when they agree with the consensus sequence and shaded according to the percentage of agreeing residues.

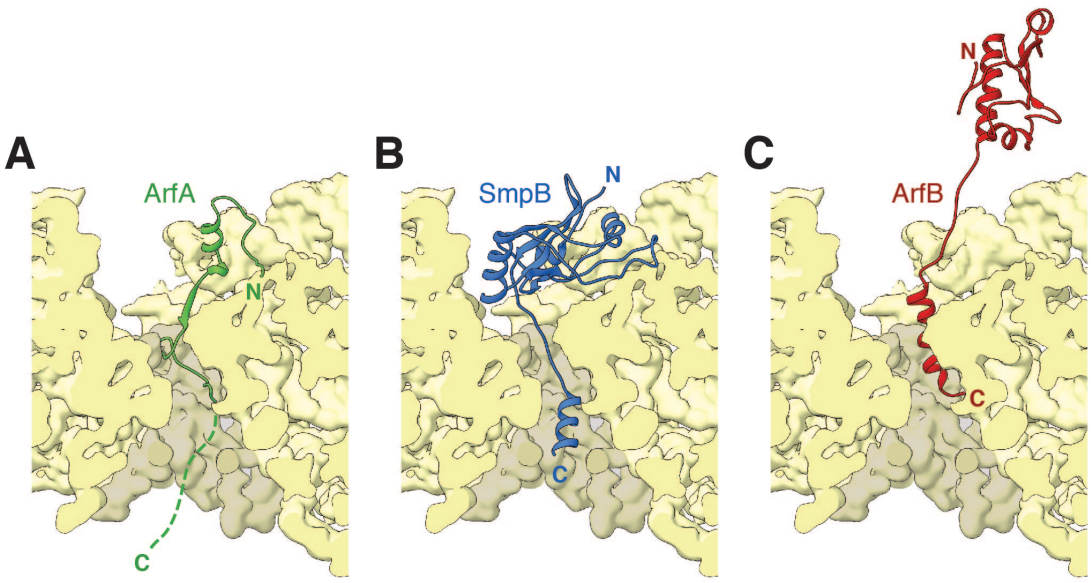

Fig. S4. ArfA, SmpB and ArfB bind the mRNA entry channel through distinct C-termini. (**A**) ArfA has an unstructured C-terminal tail that protrudes into the mRNA channel. (**B**) SmpB (PDB accession code 4V8Q) (*14*) positions a C-terminal α-helix at the entrance to the mRNA channel and has a globular N domain that binds tmRNA. (**C**) The C-terminal α-helix of ArfB (PDB accession code 4V95) (*12*) occupies the mRNA channel close to the decoding center. The globular N domain has structural homology to domain 3 of RF2 and accommodates into the PTC.

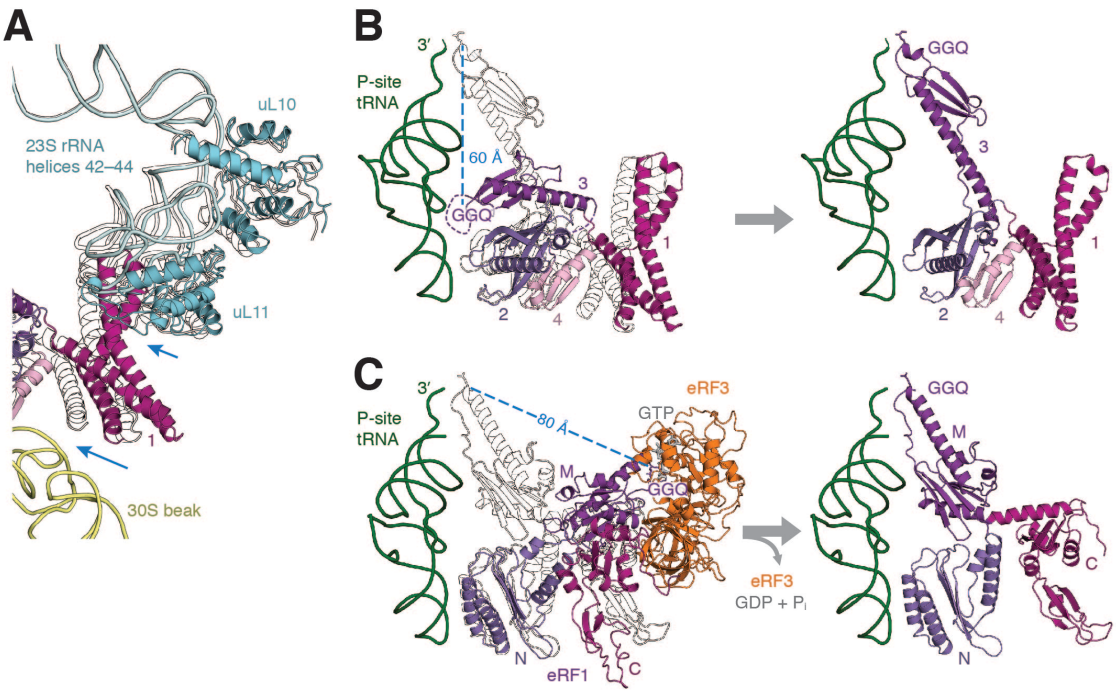

Fig. S5. Release-factor domain rearrangements. (**A**) ArfA-mediated accommodation of RF2 results in an inward movement of domain 1 together with the L7/L12 stalk base (23S rRNA helices 42–44 and the ribosomal proteins uL10 and uL11). This movement brings the three-stranded coiled coil of domain 1 into closer contact with the rRNA of the 30S beak, which may help to stabilize the accommodated state. (**B**) A superposition of pre-accommodated RF2 with accommodated RF2 (outlined) shows that all four domains move during accommodation. The GGQ loop of domain 3 rises approximately 60 Å to accommodate into the PTC. This movement is associated with a rotation of domains 2 and 4 and an inward movement of domain 1. (**C**) The conformational changes that RF2 undergoes on ArfA are analogous to those that the structurally unrelated eukaryotic release factor 1 (eRF1) undergoes on a stop codon. eRF1 is delivered to the ribosome in a pre-accommodated conformation by eRF3, a GTP-bound translational GTPase (PDB accession code 5LZT) (*28*). GTP is hydrolyzed upon stop-codon recognition and eRF3 dissociates from the ribosome. Without its GTPase partner, eRF1 changes conformation and the catalytic GGQ motif of the M domain accommodates into the PTC (PDB accession code 5LZU) (*28*).

	70S (empty A site)	70S•ArfA•RF2	70S•ArfA (A18T)•RF2	70S•ArfA•TtRF2
Data Collection				
Particles	140,027	139,792	141,950	54,465
Pixel size (Å)	1.04	1.04	1.04	1.04
Defocus mean (μm)	2.1	2.3	2.4	2.4
Defocus range (μm)	0.7–3.9	0.6–4.8	0.5–5.8	1.1–3.9
Voltage (kV)	300	300	300	300
Electron dose (e·Å^{-2})	48	48	48	48
Model composition				
Non-hydrogen atoms	146,646	149,895	149,614	149,470
Protein residues	5,971	6,379	6,344	6,321
RNA bases	4,628	4,628	4,628	4,628
Ligands (Zn^{2+}/Mg^{2+}/H_20)	2/449/2	2/453/2	2/450/2	2/462/3
Refinement				
Resolution (Å)	3.10	2.97	3.06	3.35
Map sharpening B-factor (Å^2)	−79.6	−77.0	−75.8	−91.3
Average B factor (Å^2)	95.8	75.3	99.1	85.2
$FSC_{average}$	0.89	0.90	0.89	0.85
CRef (Å)	3.1	3.0	3.1	3.4
Rms deviations				
Bond lengths (Å)	0.006	0.006	0.007	0.006
Bond angles (°)	1.08	1.10	1.16	1.20
Validation (proteins)				
MolProbity score (percentile)	2.0 (99th)	2.1 (99th)	2.2 (99th)	2.4 (98th)
Clashscore, all atoms (percentile)	2.7 (100th)	2.8 (100th)	3.2 (100th)	4.2 (100th)
Good rotamers (%)	83.0	82.2	80.9	77.1
Ramachandran plot				
Favored (%)	94.9	94.7	93.9	93.4
Outliers (%)	0.4	0.4	0.5	0.6
Validation (RNA)				
Correct sugar puckers (%)	97.8	97.9	98.2	97.8
Good backbone conformations (%)	81.4	81.3	80.8	78.8
Accession codes				
EMDB	EMD-3493	EMD-3489	EMD-3490	EMD-3492
PDB	5MDZ	5MDV	5MDW	5MDY

Table S1. Data-collection and model statistics.

References and Notes

1. K. Ito, Y. Chadani, K. Nakamori, S. Chiba, Y. Akiyama, T. Abo, Nascentome analysis uncovers futile protein synthesis in *Escherichia coli*. *PLOS ONE* **6**, e28413 (2011). doi:10.1371/journal.pone.0028413 Medline

2. K. C. Keiler, Mechanisms of ribosome rescue in bacteria. *Nat. Rev. Microbiol.* **13**, 285–297 (2015). doi:10.1038/nrmicro3438 Medline

3. E. Giudice, R. Gillet, The task force that rescues stalled ribosomes in bacteria. *Trends Biochem. Sci.* **38**, 403–411 (2013). doi:10.1016/j.tibs.2013.06.002 Medline

4. N. S. Ramadoss, J. N. Alumasa, L. Cheng, Y. Wang, S. Li, B. S. Chambers, H. Chang, A. K. Chatterjee, A. Brinker, I. H. Engels, K. C. Keiler, Small molecule inhibitors of trans-translation have broad-spectrum antibiotic activity. *Proc. Natl. Acad. Sci. U.S.A.* **110**, 10282–10287 (2013). doi:10.1073/pnas.1302816110 Medline

5. Y. Chadani, K. Ono, S. Ozawa, Y. Takahashi, K. Takai, H. Nanamiya, Y. Tozawa, K. Kutsukake, T. Abo, Ribosome rescue by *Escherichia coli* ArfA (YhdL) in the absence of trans-translation system. *Mol. Microbiol.* **78**, 796–808 (2010). doi:10.1111/j.1365-2958.2010.07375.x Medline

6. Y. Komine, M. Kitabatake, T. Yokogawa, K. Nishikawa, H. Inokuchi, A tRNA-like structure is present in 10Sa RNA, a small stable RNA from *Escherichia coli*. *Proc. Natl. Acad. Sci. U.S.A.* **91**, 9223–9227 (1994). doi:10.1073/pnas.91.20.9223 Medline

7. Y. Chadani, E. Matsumoto, H. Aso, T. Wada, K. Kutsukake, S. Sutou, T. Abo, trans-translation-mediated tight regulation of the expression of the alternative ribosome-rescue factor ArfA in *Escherichia coli*. *Genes Genet. Syst.* **86**, 151–163 (2011). doi:10.1266/ggs.86.151 Medline

8. F. Garza-Sánchez, R. E. Schaub, B. D. Janssen, C. S. Hayes, tmRNA regulates synthesis of the ArfA ribosome rescue factor. *Mol. Microbiol.* **80**, 1204–1219 (2011). doi:10.1111/j.1365-2958.2011.07638.x Medline

9. R. E. Schaub, S. J. Poole, F. Garza-Sánchez, S. Benbow, C. S. Hayes, Proteobacterial ArfA peptides are synthesized from non-stop messenger RNAs. *J. Biol. Chem.* **287**, 29765–29775 (2012). doi:10.1074/jbc.M112.374074 Medline

10. Y. Chadani, K. Ito, K. Kutsukake, T. Abo, ArfA recruits release factor 2 to rescue stalled ribosomes by peptidyl-tRNA hydrolysis in *Escherichia coli*. *Mol. Microbiol.* **86**, 37–50 (2012). doi:10.1111/j.1365-2958.2012.08190.x Medline

11. Y. Shimizu, ArfA recruits RF2 into stalled ribosomes. *J. Mol. Biol.* **423**, 624–631 (2012). doi:10.1016/j.jmb.2012.08.007 Medline

12. M. G. Gagnon, S. V. Seetharaman, D. Bulkley, T. A. Steitz, Structural basis for the rescue of stalled ribosomes: Structure of YaeJ bound to the ribosome. *Science* **335**, 1370–1372 (2012). doi:10.1126/science.1217443 Medline

13. D. Kurita, Y. Chadani, A. Muto, T. Abo, H. Himeno, ArfA recognizes the lack of mRNA in the mRNA channel after RF2 binding for ribosome rescue. *Nucleic Acids Res.* **42**, 13339–13352 (2014). doi:10.1093/nar/gku1069 Medline

14. C. Neubauer, R. Gillet, A. C. Kelley, V. Ramakrishnan, Decoding in the absence of a codon by tmRNA and SmpB in the ribosome. *Science* **335**, 1366–1369 (2012). doi:10.1126/science.1217039 Medline

15. F. Zeng, H. Jin, Peptide release promoted by methylated RF2 and ArfA in nonstop translation is achieved by an induced-fit mechanism. *RNA* **22**, 49–60 (2016). doi:10.1261/rna.053082.115 Medline

16. A. Weixlbaumer *et al*., Insights into translational termination from the structure of RF2 bound to the ribosome. *Science* **322**, 953–956 (2008). doi:10.1126/science.1164840 Medline

17. U. B. S. Rawat, A. V. Zavialov, J. Sengupta, M. Valle, R. A. Grassucci, J. Linde, B. Vestergaard, M. Ehrenberg, J. Frank, A cryo-electron microscopic study of ribosome-bound termination factor RF2. *Nature* **421**, 87–90 (2003). doi:10.1038/nature01224 Medline

18. B. P. Klaholz, T. Pape, A. V. Zavialov, A. G. Myasnikov, E. V. Orlova, B. Vestergaard, M. Ehrenberg, M. van Heel, Structure of the *Escherichia coli* ribosomal termination complex with release factor 2. *Nature* **421**, 90–94 (2003). doi:10.1038/nature01225 Medline

19. M. Laurberg, H. Asahara, A. Korostelev, J. Zhu, S. Trakhanov, H. F. Noller, Structural basis for translation termination on the 70S ribosome. *Nature* **454**, 852–857 (2008). doi:10.1038/nature07115 Medline

20. A. Korostelev, H. Asahara, L. Lancaster, M. Laurberg, A. Hirschi, J. Zhu, S. Trakhanov, W. G. Scott, H. F. Noller, Crystal structure of a translation termination complex formed with release factor RF2. *Proc. Natl. Acad. Sci. U.S.A.* **105**, 19684–19689 (2008). doi:10.1073/pnas.0810953105 Medline

21. B. Vestergaard, L. B. Van, G. R. Andersen, J. Nyborg, R. H. Buckingham, M. Kjeldgaard, Bacterial polypeptide release factor RF2 is structurally distinct from eukaryotic eRF1. *Mol. Cell* **8**, 1375–1382 (2001). doi:10.1016/S1097-2765(01)00415-4 Medline

22. D. H. Shin, J. Brandsen, J. Jancarik, H. Yokota, R. Kim, S.-H. Kim, Structural analyses of peptide release factor 1 from *Thermotoga maritima* reveal domain flexibility required for its interaction with the ribosome. *J. Mol. Biol.* **341**, 227–239 (2004). doi:10.1016/j.jmb.2004.05.055 Medline

23. G. Zoldák, L. Redecke, D. I. Svergun, P. V. Konarev, C. S. Voertler, H. Dobbek, E. Sedlák, M. Sprinzl, Release factors 2 from *Escherichia coli* and *Thermus thermophilus*: Structural, spectroscopic and microcalorimetric studies. *Nucleic Acids Res.* **35**, 1343–1353 (2007). doi:10.1093/nar/gkl696 Medline

24. B. Vestergaard, S. Sanyal, M. Roessle, L. Mora, R. H. Buckingham, J. S. Kastrup, M. Gajhede, D. I. Svergun, M. Ehrenberg, The SAXS solution structure of RF1 differs from its crystal structure and is similar to its ribosome bound cryo-EM structure. *Mol. Cell* **20**, 929–938 (2005). doi:10.1016/j.molcel.2005.11.022 Medline

25. S. L. He, R. Green, Visualization of codon-dependent conformational rearrangements during translation termination. *Nat. Struct. Mol. Biol.* **17**, 465–470 (2010). doi:10.1038/nsmb.1766 Medline

26. K. Trappl, S. Joseph, Ribosome induces a closed to open conformational change in release factor 1. *J. Mol. Biol.* **428**, 1333–1344 (2016). doi:10.1016/j.jmb.2016.01.021 Medline

27. R. M. Voorhees, V. Ramakrishnan, Structural basis of the translational elongation cycle. *Annu. Rev. Biochem.* **82**, 203–236 (2013). doi:10.1146/annurev-biochem-113009-092313 Medline

28. S. Shao, J. Murray, A. Brown, J. Taunton, V. Ramakrishnan, R. S. Hegde, Decoding mammalian tibosome-mRNA states by translational GTPase complexes. *Cell* **167**, 1229–1240 (2016). doi:10.1016/j.cell.2016.10.046

29. B. Hetrick, K. Lee, S. Joseph, Kinetics of stop codon recognition by release factor 1. *Biochemistry* **48**, 11178–11184 (2009). doi:10.1021/bi901577d Medline

30. D. V. Freistroffer, M. Kwiatkowski, R. H. Buckingham, M. Ehrenberg, The accuracy of codon recognition by polypeptide release factors. *Proc. Natl. Acad. Sci. U.S.A.* **97**, 2046–2051 (2000). doi:10.1073/pnas.030541097 Medline

31. A. Brown, I. S. Fernández, Y. Gordiyenko, V. Ramakrishnan, Ribosome-dependent activation of stringent control. *Nature* **534**, 277–280 (2016). Medline

32. Y. Shimizu, A. Inoue, Y. Tomari, T. Suzuki, T. Yokogawa, K. Nishikawa, T. Ueda, Cell-free translation reconstituted with purified components. *Nat. Biotechnol.* **19**, 751–755 (2001). doi:10.1038/90802 Medline

33. R. M. Voorhees, A. Weixlbaumer, D. Loakes, A. C. Kelley, V. Ramakrishnan, Insights into substrate stabilization from snapshots of the peptidyl transferase center of the intact 70S ribosome. *Nat. Struct. Mol. Biol.* **16**, 528–533 (2009). doi:10.1038/nsmb.1577 Medline

34. M. Selmer, C. M. Dunham, F. V. Murphy 4th, A. Weixlbaumer, S. Petry, A. C. Kelley, J. R. Weir, V. Ramakrishnan, Structure of the 70S ribosome complexed with mRNA and tRNA. *Science* **313**, 1935–1942 (2006). doi:10.1126/science.1131127 Medline

35. X. Li, P. Mooney, S. Zheng, C. R. Booth, M. B. Braunfeld, S. Gubbens, D. A. Agard, Y. Cheng, Electron counting and beam-induced motion correction enable near-atomic-resolution single-particle cryo-EM. *Nat. Methods* **10**, 584–590 (2013). doi:10.1038/nmeth.2472 Medline

36. K. Zhang, Gctf: Real-time CTF determination and correction. *J. Struct. Biol.* **193**, 1–12 (2016). doi:10.1016/j.jsb.2015.11.003 Medline

37. R. Fernandez-Leiro, S. Scheres, A pipeline approach to single-particle processing in RELION. *bioRxiv* (2016). 10.1101/078352

38. S. H. W. Scheres, Semi-automated selection of cryo-EM particles in RELION-1.3. *J. Struct. Biol.* **189**, 114–122 (2015). doi:10.1016/j.jsb.2014.11.010 Medline

39. X.-C. Bai, E. Rajendra, G. Yang, Y. Shi, S. H. Scheres, Sampling the conformational space of the catalytic subunit of human γ-secretase. *eLife* **4**, 1485 (2015). doi:10.7554/eLife.11182

40. P. B. Rosenthal, R. Henderson, Optimal determination of particle orientation, absolute hand, and contrast loss in single-particle electron cryomicroscopy. *J. Mol. Biol.* **333**, 721–745 (2003). doi:10.1016/j.jmb.2003.07.013 Medline

41. S. Chen, G. McMullan, A. R. Faruqi, G. N. Murshudov, J. M. Short, S. H. W. Scheres, R. Henderson, High-resolution noise substitution to measure overfitting and validate resolution in 3D structure determination by single particle electron cryomicroscopy. *Ultramicroscopy* **135**, 24–35 (2013). doi:10.1016/j.ultramic.2013.06.004 Medline

42. A. Kucukelbir, F. J. Sigworth, H. D. Tagare, Quantifying the local resolution of cryo-EM density maps. *Nat. Methods* **11**, 63–65 (2014). doi:10.1038/nmeth.2727 Medline

43. E. F. Pettersen, T. D. Goddard, C. C. Huang, G. S. Couch, D. M. Greenblatt, E. C. Meng, T. E. Ferrin, UCSF Chimera—A visualization system for exploratory research and analysis. *J. Comput. Chem.* **25**, 1605–1612 (2004). doi:10.1002/jcc.20084 Medline

44. P. Emsley, B. Lohkamp, W. G. Scott, K. Cowtan, Features and development of *Coot*. *Acta Crystallogr. D* **66**, 486–501 (2010). doi:10.1107/S0907444910007493 Medline

45. A. Brown, F. Long, R. A. Nicholls, J. Toots, P. Emsley, G. Murshudov, Tools for macromolecular model building and refinement into electron cryo-microscopy reconstructions. *Acta Crystallogr. D* **71**, 136–153 (2015). doi:10.1107/S1399004714021683 Medline

46. V. B. Chen, W. B. Arendall III, J. J. Headd, D. A. Keedy, R. M. Immormino, G. J. Kapral, L. W. Murray, J. S. Richardson, D. C. Richardson, MolProbity: All-atom structure validation for macromolecular crystallography. *Acta Crystallogr. D* **66**, 12–21 (2010). doi:10.1107/S0907444909042073 Medline

47. W. L. DeLano, The PyMOL molecular graphics system (2002).

48. UniProt Consortium, UniProt: A hub for protein information. *Nucleic Acids Res.* **43**, D204–D212 (2015). doi:10.1093/nar/gku989 Medline

49. R. C. Edgar, MUSCLE: Multiple sequence alignment with high accuracy and high throughput. *Nucleic Acids Res.* **32**, 1792–1797 (2004). doi:10.1093/nar/gkh340 Medline

50. A. M. Waterhouse, J. B. Procter, D. M. A. Martin, M. Clamp, G. J. Barton, Jalview version 2—A multiple sequence alignment editor and analysis workbench. *Bioinformatics* **25**, 1189–1191 (2009). Medline